A Sparsity Approach for Near-Field Antenna Characterization with Truncation Error

M. Salucci, N. Anselmi, and A. Massa

2024/05/17

Contents

1 Fixed measurement step $\Delta_z^{meas} = 1\,[\lambda]$ and different number of measurement points (M) and same number of estimated coefficients for both *BCS-MbD & OMP-MbD*

The main goal of this section is to compare the performance of the *OMP* and *BCS* solvers when the same number of estimated coefficients are considered. In particular, given the *BCS* solution, the *OMP* iteration to show is chosen according to the number of indexes selected by the *BCS* algorithm.

1.0.1 Height of the measurement region $H_{meas} = 5\,[\lambda]$

Near-Field Error

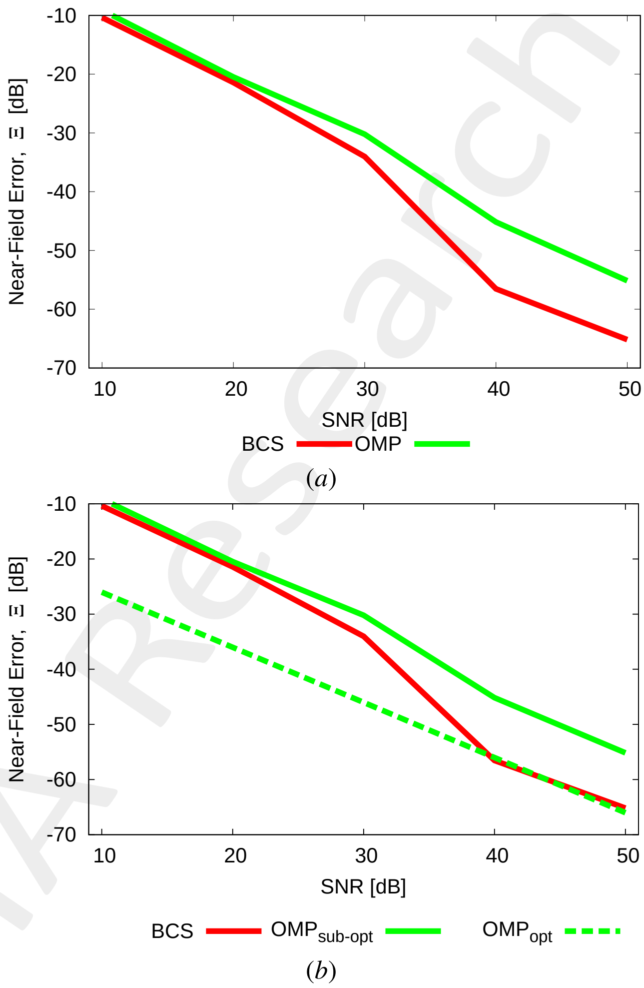

Figure 1: (*a*) Near-field error comparison between original (*OMP*) and alternative (*BCS*) MbD for different SNR values when the same number of coefficients are considered for both *OMP* and *BCS*; (*b*) Comparison between near-field error (*a*) and the case in which the optimal *OMP* iteration is considered.

$SNR\,[dB]$	*Near Field Error,* Ξ $[dB]$	
	BCS	OMP
50	-65.18	-55.15
40	-56.53	-45.15
30	-34.03	-30.21
20	-21.42	-20.48
10	-10.35	-9.12

Table I: Near Field Errors obtained by the original (*OMP*) and alternative (*BCS*) MbD

Observations

By observing the reported results, it is possible to point out that the consideration of a number of *OMP* coefficients (i.e. considered *OMP* iteration) equal to that of the *BCS* results in a degradation of the *OMP* performance so that the *BCS* near-field error is always lower than that of the *OMP* solver.

Estimated Coefficients

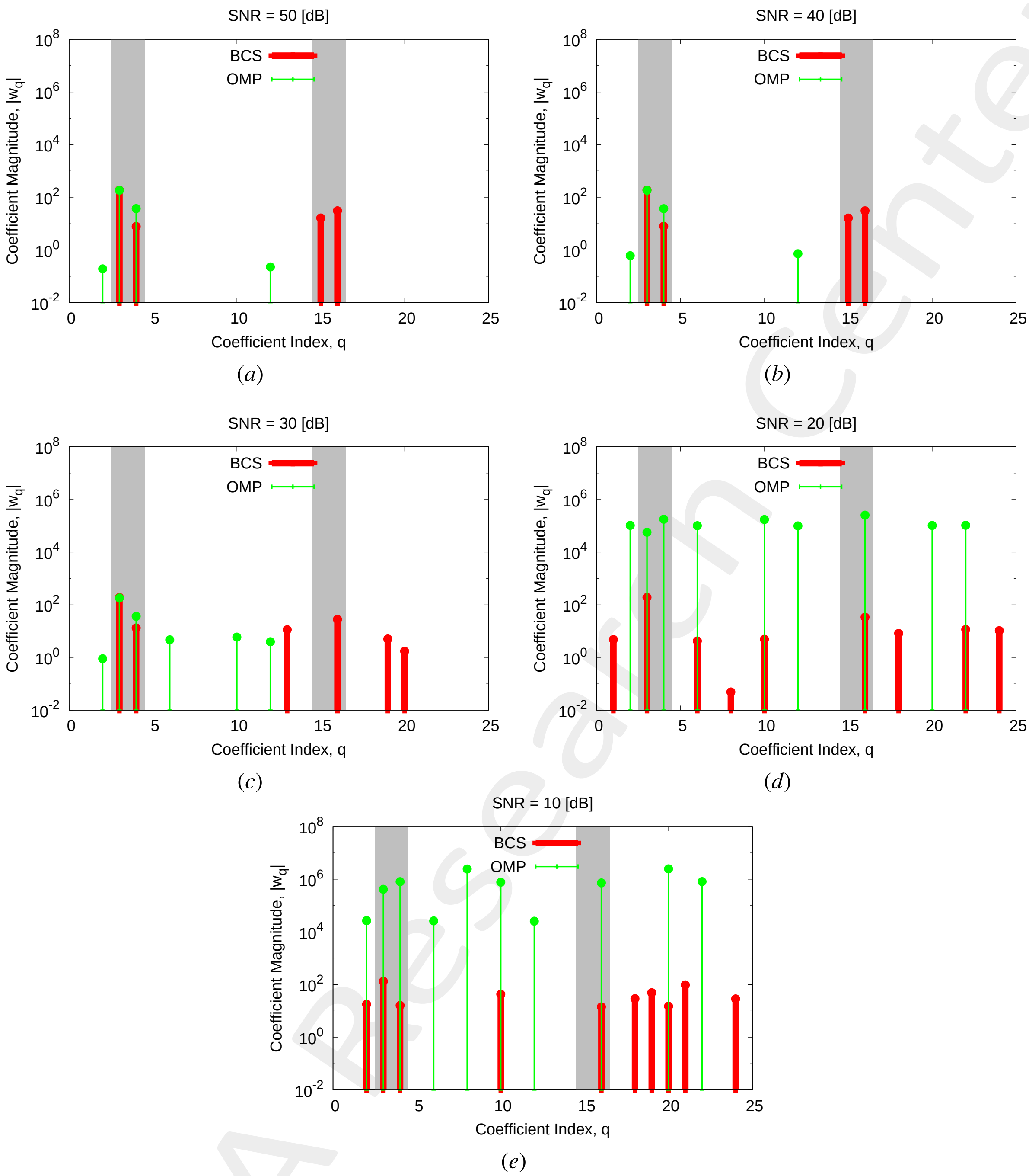

Figure 2: Coefficient comparison between original (*OMP*) and alternative (*BCS*) MbD : (*a*) $SNR = 50\,[dB]$, (*b*) $SNR = 40\,[dB]$, (*c*) $SNR = 30\,[dB]$, (*d*) $SNR = 20\,[dB]$, (*e*) $SNR = 10\,[dB]$

Observations

The considered *AUT* is characterized by an excitation magnitude and phase of the second subarray (i.e., $\nu^{(2)} = 0.43$ and $\gamma^{(2)} = \frac{\pi}{3}\,[rad]$):

- the *OMP* algorithm is able to identify at least one failure affecting the AUT even if the failure detections are not precise since the method selects also vectors not connected to the actual failures and it doesn't pick all the vectors of the failures affecting the *AUT;*
- the *BCS* algorithm is able to identify both the failures affecting the AUT even if the failure detections, at $10\,[dB] \leq$

$SNR \leq 30\,[dB]$, are not precise since the method selects also vectors not connected to the actual failures and it doesn't pick all the vectors of the failures affecting the *AUT*. For $SNR \geq 40\,[dB]$ the BCS precisely selects all the basis functions associated to the failures affecting the *AUT*.

1.0.2 Height of the measurement region $\mathbf{H_{meas}} = 4\,[\lambda]$

Near-Field Error

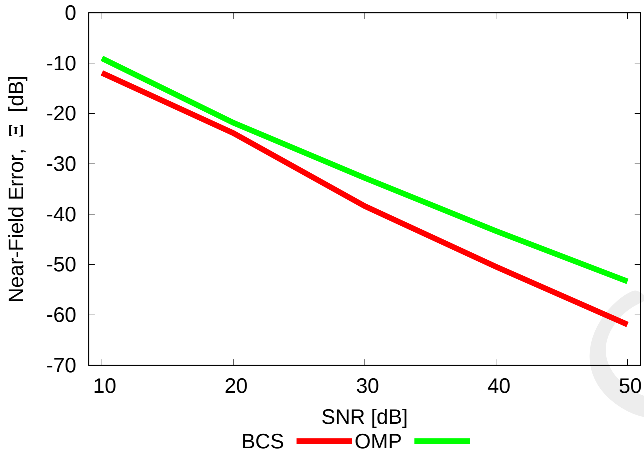

(a)

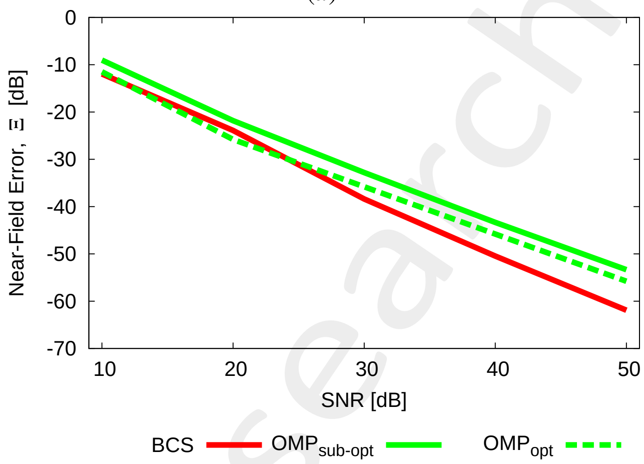

(b)

Figure 3: (a) Near-field error comparison between original (*OMP*) and alternative (*BCS*) MbD for different SNR values when the same number of coefficients are considered for both *OMP* and *BCS*; (b) Comparison between near-field error (a) and the case in which the optimal *OMP* iteration is considered.

$SNR\,[dB]$	*Near Field Error,* Ξ $[dB]$	
	BCS	OMP
50	-61.91	-53.34
40	-50.45	-43.35
30	-38.39	-32.81
20	-23.87	-21.83
10	-11.94	-9.03

Table II: Near Field Errors obtained by the original (*OMP*) and alternative (*BCS*) MbD

Observations

By observing the reported results, it is possible to point out that the consideration of a number of *OMP* coefficients (i.e. considered *OMP* iteration) equal to that of the *BCS* results in a degradation of the *OMP* performance so that the *BCS* near-field error is always lower than that of the *OMP* solver.

Estimated Coefficients

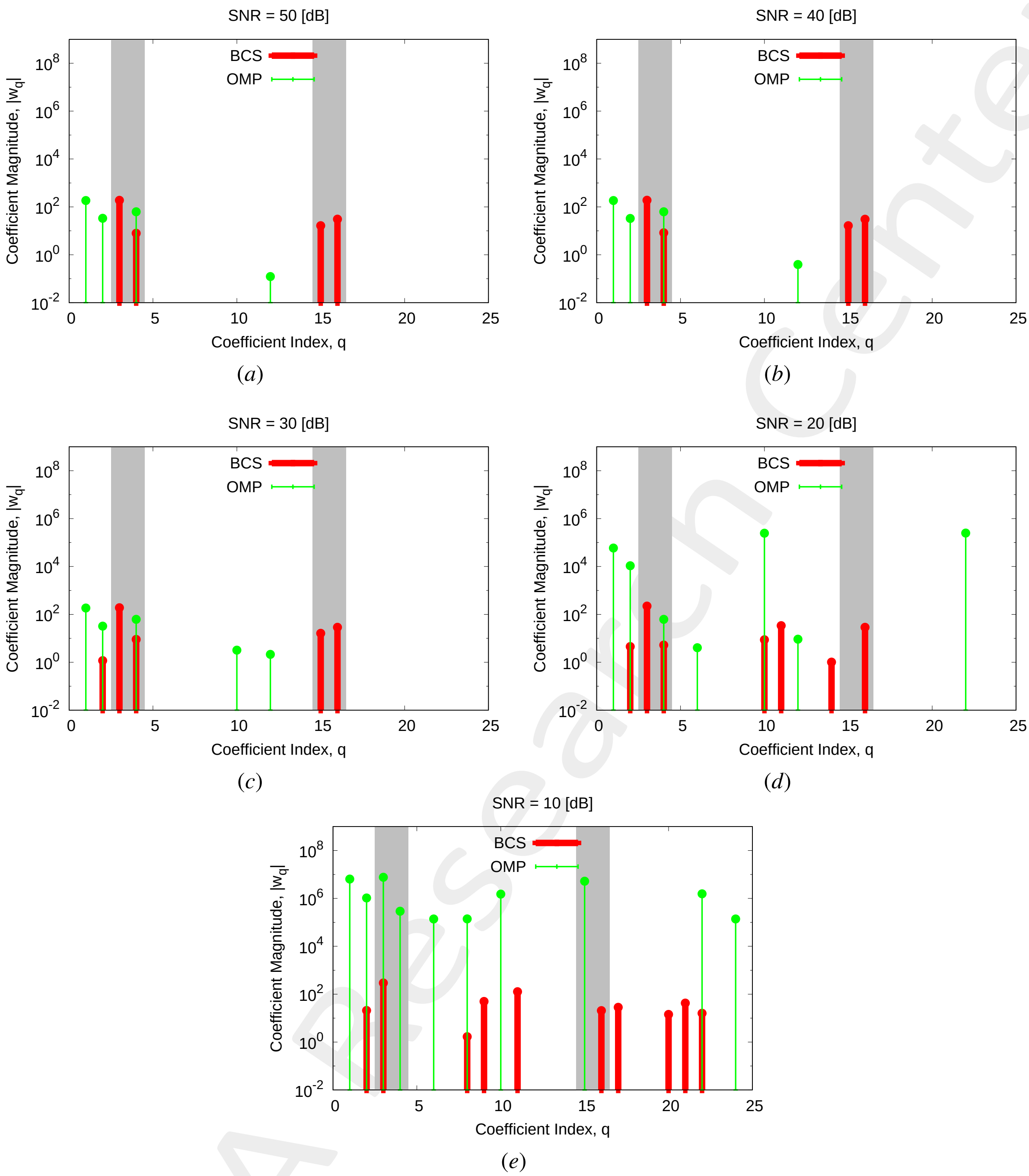

Figure 4: Coefficient comparison between original (*OMP*) and alternative (*BCS*) MbD : (*a*) $SNR = 50\,[dB]$, (*b*) $SNR = 40\,[dB]$, (*c*) $SNR = 30\,[dB]$, (*d*) $SNR = 20\,[dB]$, (*e*) $SNR = 10\,[dB]$

Observations

The considered *AUT* is characterized by an excitation magnitude and phase of the second subarray (i.e., $\nu^{(2)} = 0.43$ and $\gamma^{(2)} = \frac{\pi}{3}\,[rad]$):

- the *OMP* algorithm is able to identify at least one failure affecting the AUT even if the failure detections are not precise since the method selects also vectors not connected to the actual failures and it doesn't pick all the vectors of the failures affecting the *AUT;*
- the *BCS* algorithm is able to identify both the failures affecting the AUT even if the failure detections are not

precise at low $SNRs$ since the method selects also vectors not connected to the actual failures and it doesn't pick all the vectors of the failures affecting the *AUT*. In particular, the *BCS* correctly identify both the failures affecting the *AUT* starting from $SNR = 40\,[dB]$.

1.0.3 Height of the measurement region $\mathbf{H_{meas} = 3}\,[\lambda]$

Near-Field Error

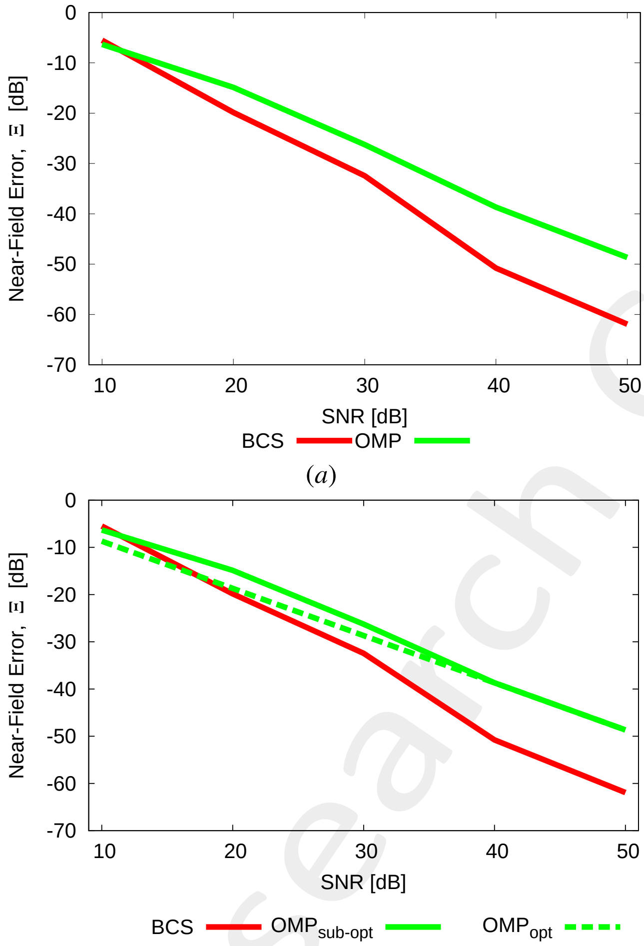

(*a*)

(*b*)

Figure 5: (*a*) Near-field error comparison between original (*OMP*) and alternative (*BCS*) MbD for different SNR values when the same number of coefficients are considered for both *OMP* and *BCS*; (*b*) Comparison between near-field error (*a*) and the case in which the optimal *OMP* iteration is considered.

$SNR\,[dB]$	*Near Field Error,* $\Xi\ [dB]$	
	BCS	OMP
50	-61.93	-48.67
40	-50.78	-38.68
30	-32.44	-26.26
20	-19.85	-14.88
10	-5.49	-6.33

Table III: Near Field Errors obtained by the original (*OMP*) and alternative (*BCS*) MbD

Observations

By observing the reported results, it is possible to point out that the consideration of a number of *OMP* coefficients (i.e. considered *OMP* iteration) equal to that of the *BCS* results in a degradation of the *OMP* performance so that the *BCS* near-field error is almost always lower than that of the *OMP* solver.

Estimated Coefficients

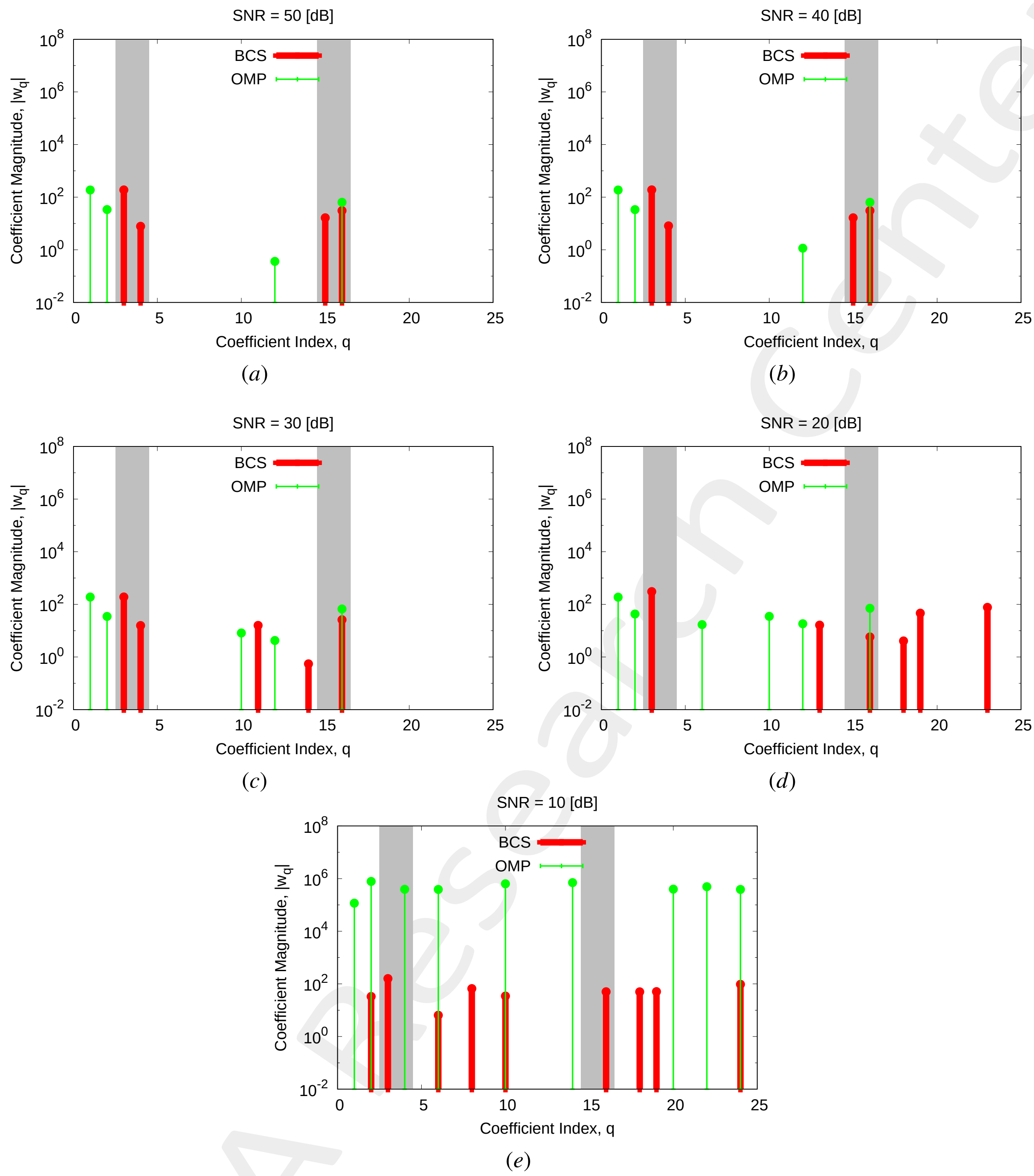

Figure 6: Coefficient comparison between original (*OMP*) and alternative (*BCS*) MbD : (*a*) $SNR = 50\,[dB]$, (*b*) $SNR = 40\,[dB]$, (*c*) $SNR = 30\,[dB]$, (*d*) $SNR = 20\,[dB]$, (*e*) $SNR = 10\,[dB]$

Observations

The considered *AUT* is characterized by an excitation magnitude and phase of the second subarray (i.e., $\nu^{(2)} = 0.43$ and $\gamma^{(2)} = \frac{\pi}{3}\,[rad]$)

- the *OMP* solver selects vectors associated to both magnitude and phase failures and is always able to identify at least one failure affecting the *AUT*.
- the *BCS* algorithm is able to identify both the failures affecting the AUT even if the failure detections are not precise since the method selects also vectors not connected to the actual failures and it doesn't pick all the vectors

of the failures affecting the *AUT*. In particular, the *BCS* precisely identify both the failures affecting the AUT only at $SNR = 40\,[dB]$.

1.0.4 Height of the measurement region $\mathbf{H_{meas}} = \mathbf{2}\,[\lambda]$

Near-Field Error

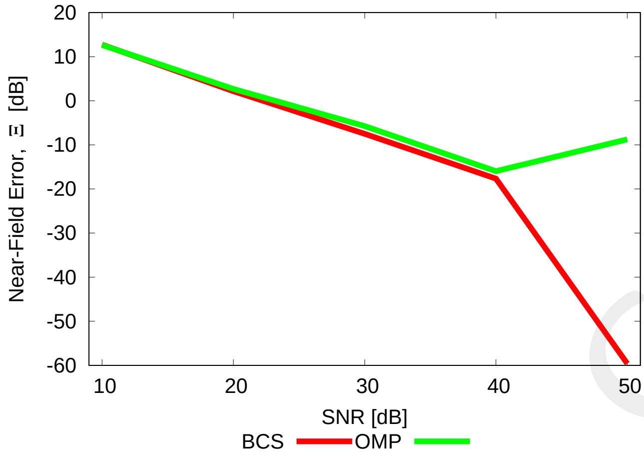

(*a*)

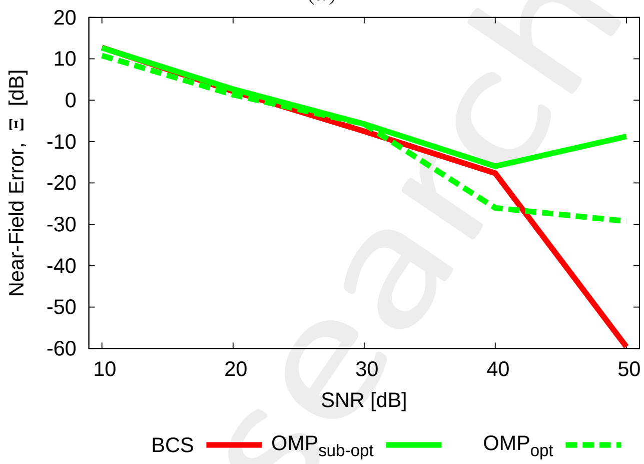

(*b*)

Figure 7: (*a*) Near-field error comparison between original (*OMP*) and alternative (*BCS*) MbD for different SNR values when the same number of coefficients are considered for both *OMP* and *BCS*; (*b*) Comparison between near-field error (*a*) and the case in which the optimal *OMP* iteration is considered.

$SNR\,[dB]$	*Near Field Error,* Ξ $[dB]$	
	BCS	OMP
50	-59.59	-8.76
40	-17.65	-15.97
30	-7.51	-5.76
20	2.17	2.67
10	12.74	12.65

Table IV: Near Field Errors obtained by the original (*OMP*) and alternative (*BCS*) MbD

Observations

By observing the reported results, it is possible to point out that the consideration of a number of *OMP* coefficients (i.e. considered *OMP* iteration) equal to that of the *BCS* results in a degradation of the *OMP* performance so that the *BCS* near-field error is almost always lower than that of the *OMP* solver.

Estimated Coefficients

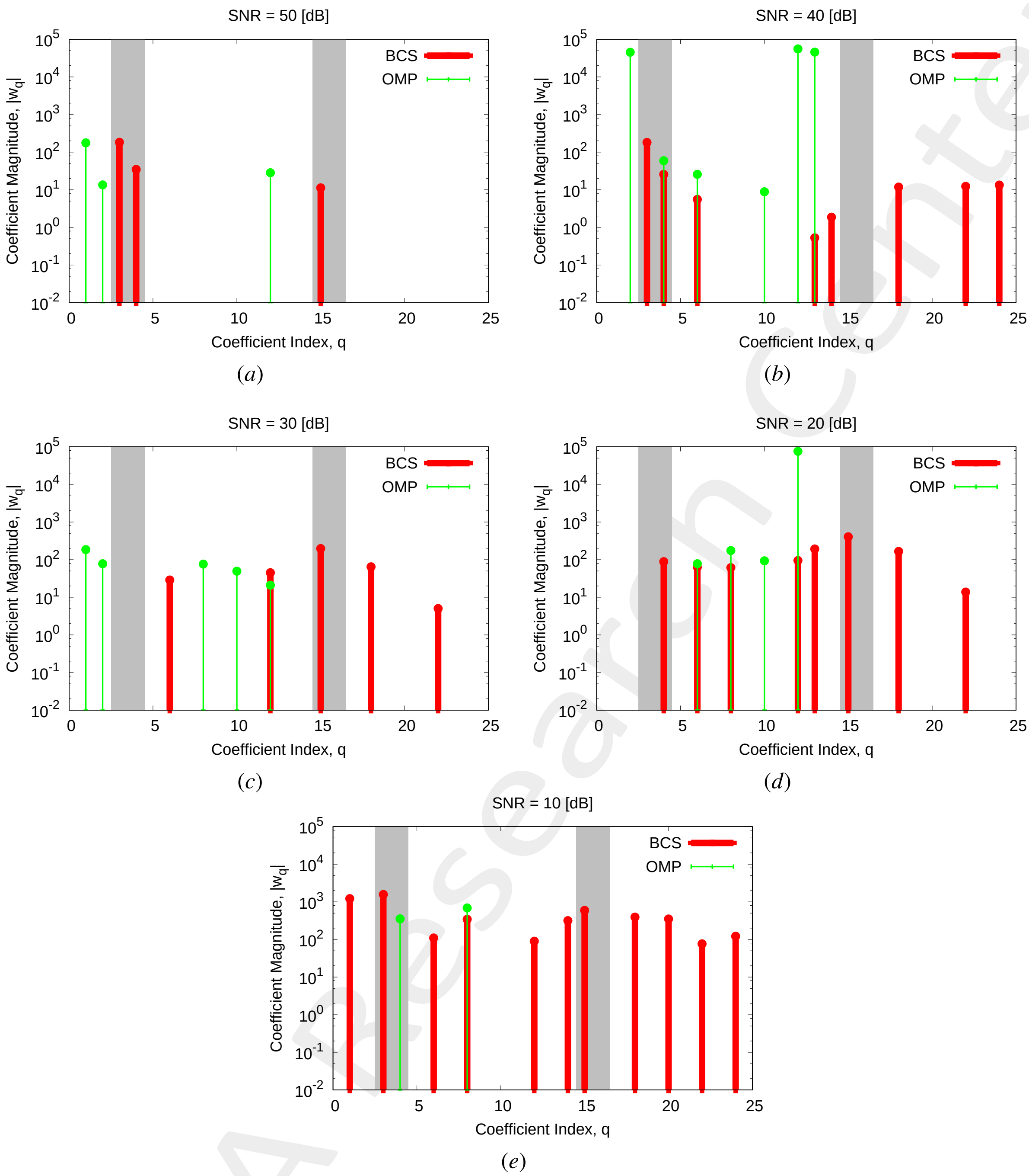

Figure 8: Coefficient comparison between original (*OMP*) and alternative (*BCS*) MbD : (*a*) $SNR = 50\,[dB]$, (*b*) $SNR = 40\,[dB]$, (*c*) $SNR = 30\,[dB]$, (*d*) $SNR = 20\,[dB]$, (*e*) $SNR = 10\,[dB]$

Observations

The considered *AUT* is characterized by an excitation magnitude and phase of the second subarray (i.e., $\nu^{(2)} = 0.43$ and $\gamma^{(2)} = \frac{\pi}{3}\,[rad]$):

- the *OMP* solver selects vectors associated to both magnitude and phase failures and in some cases is able to identify the magnitude failure affecting the *AUT*.
- the *BCS* algorithm is able to identify at least one failure affecting the AUT even if the failure detections are not precise since the method selects also vectors not connected to the actual failures and it doesn't pick all the vectors

of the failures affecting the *AUT*. At $SNR = 50\,[dB]$ the *BCS* solver precisely identifies both the failures affecting the *AUT*.

1.0.5 Height of the measurement region $\mathbf{H_{meas}} = \mathbf{1}\,[\lambda]$

Near-Field Error

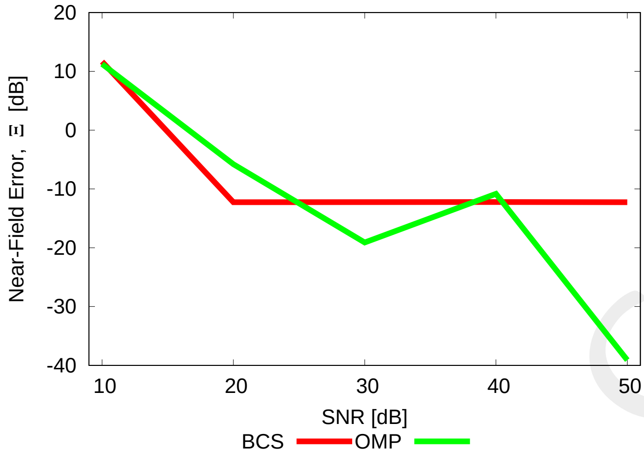

(*a*)

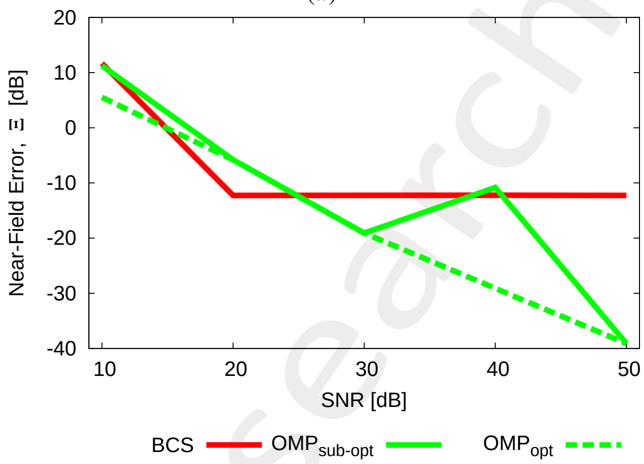

(*b*)

Figure 9: (*a*) Near-field error comparison between original (*OMP*) and alternative (*BCS*) MbD for different SNR values when the same number of coefficients are considered for both *OMP* and *BCS*; (*b*) Comparison between near-field error (*a*) and the case in which the optimal *OMP* iteration is considered.

$SNR\,[dB]$	*Near Field Error,* $\Xi\,[dB]$	
	BCS	OMP
50	-12.26	-39.10
40	-12.22	-10.83
30	-12.23	-19.10
20	-12.26	-5.79
10	11.66	11.25

Table V: Near Field Errors obtained by the original (*OMP*) and alternative (*BCS*) MbD

Observations

By observing the reported results, it is possible to point out that the consideration of a number of *OMP* coefficients (i.e. considered *OMP* iteration) equal to that of the *BCS* results in a degradation of the *OMP* performance; nevertheless, both solvers achieve errors that do not allow a good near-field reconstruction, except the case $SNR = 50\,[dB]$ for the *OMP*.

Estimated Coefficients

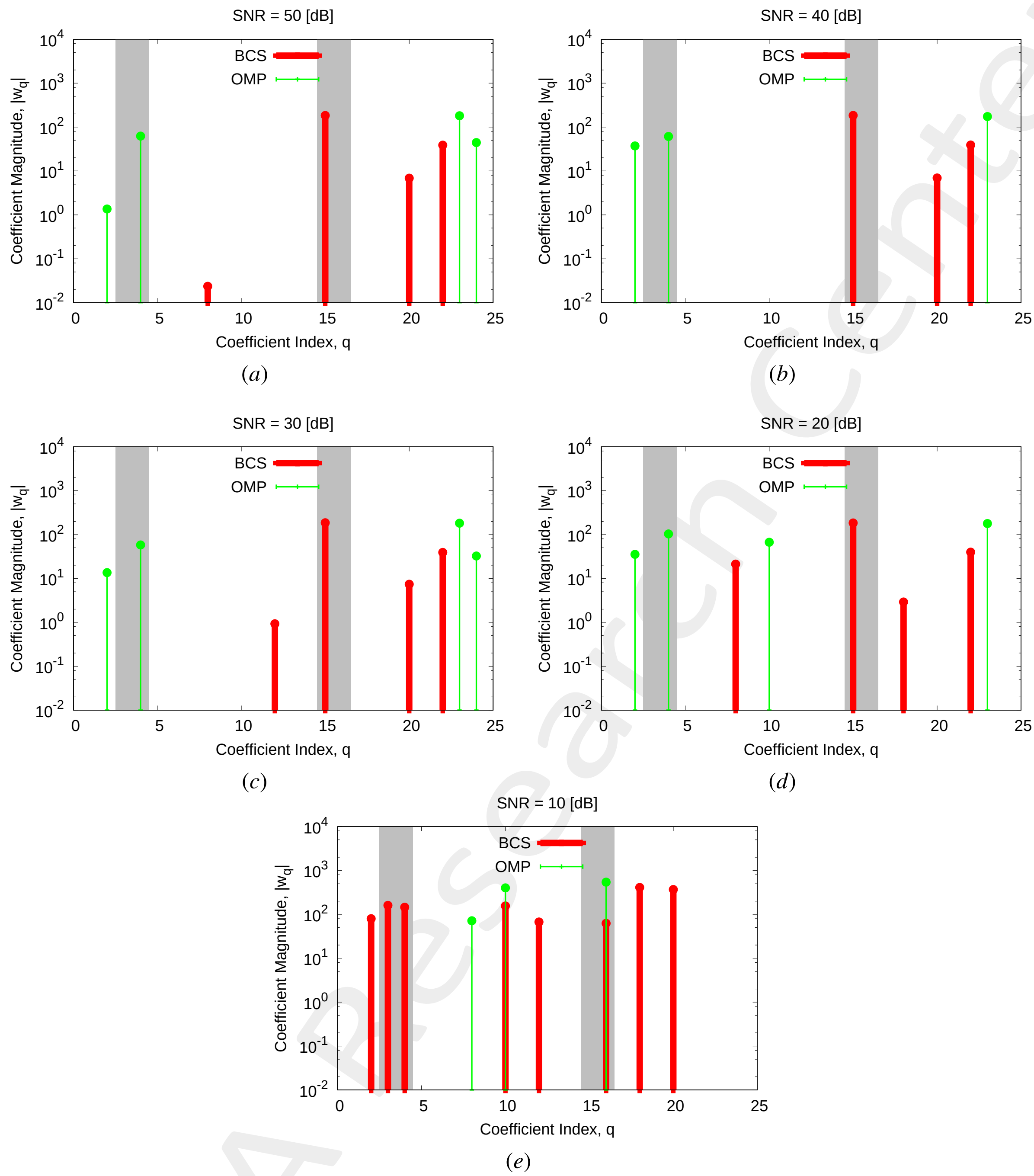

Figure 10: Coefficient comparison between original (*OMP*) and alternative (*BCS*) MbD : (*a*) $SNR = 50\,[dB]$, (*b*) $SNR = 40\,[dB]$, (*c*) $SNR = 30\,[dB]$, (*d*) $SNR = 20\,[dB]$, (*e*) $SNR = 10\,[dB]$

Observations

The considered *AUT* is characterized by an excitation magnitude and phase of the second subarray (i.e., $\nu^{(2)} = 0.43$ and $\gamma^{(2)} = \frac{\pi}{3}\,[rad]$):

- the *OMP* algorithm is able to identify at least one failure affecting the AUT even if the failure detections are not precise since the method selects also vectors not connected to the actual failures and it doesn't pick all the vectors of the failures affecting the *AUT;*
- the *BCS* solver selects vectors associated to both magnitude and phase failures

- and identifies only the phase failure affecting the *AUT*.

More information on the topics of this document can be found in the following list of references.

References

[1] M. Salucci, N. Anselmi, M. D. Migliore and A. Massa, "A bayesian compressive sensing approach to robust near-field antenna characterization," *IEEE Trans. Antennas Propag.*, vol. 70, no. 9, pp. 8671-8676, Sep. 2022 (DOI: 10.1109/TAP.2022.3177528).

[2] B. Li, M. Salucci, W. Tang, and P. Rocca, "Reliable field strength prediction through an adaptive total-variation CS technique," *IEEE Antennas Wirel. Propag. Lett.*, vol. 19, no. 9, pp. 1566-1570, Sep. 2020.

[3] M. Salucci, M. D. Migliore, P. Rocca, A. Polo, and A. Massa, "Reliable antenna measurements in a near-field cylindrical setup with a sparsity promoting approach," *IEEE Trans. Antennas Propag.*, vol. 68, no. 5, pp. 4143-4148, May 2020.

[4] G. Oliveri, M. Salucci, N. Anselmi, and A. Massa, "Compressive sensing as applied to inverse problems for imaging: theory, applications, current trends, and open challenges," *IEEE Antennas Propag. Mag. - Special Issue on "Electromagnetic Inverse Problems for Sensing and Imaging*," vol. 59, no. 5, pp. 34-46, Oct. 2017.

[5] A. Massa, P. Rocca, and G. Oliveri, "Compressive sensing in electromagnetics - A review," *IEEE Antennas Propag. Mag.*, pp. 224-238, vol. 57, no. 1, Feb. 2015.

[6] A. Massa and F. Texeira, "Guest-Editorial: Special Cluster on Compressive Sensing as Applied to Electromagnetics," *IEEE Antennas Wirel. Propag. Lett.*, vol. 14, pp. 1022-1026, 2015.

[7] G. Oliveri, N. Anselmi, M. Salucci, L. Poli, and A. Massa, "Compressive sampling-based scattering data acquisition in microwave imaging," *J. Electromagn. Waves Appl*, vol. 37, no. 5, 693-729, March 2023 (DOI: 10.1080/09205071.2023.2188263).

[8] G. Oliveri, L. Poli, N. Anselmi, M. Salucci, and A. Massa, "Compressive sensing-based Born iterative method for tomographic imaging," *IEEE Trans. Microw. Theory Techn.*, vol. 67, no. 5, pp. 1753-1765, May 2019.

[9] M. Salucci, L. Poli, and G. Oliveri, "Full-vectorial 3D microwave imaging of sparse scatterers through a multi-task Bayesian compressive sensing approach," *J. Imaging*, vol. 5, no. 1, pp. 1-24, Jan. 2019.

[10] M. Salucci, A. Gelmini, L. Poli, G. Oliveri, and A. Massa, "Progressive compressive sensing for exploiting frequency-diversity in GPR imaging," *J. Electromagn. Waves Appl.*, vol. 32, no. 9, pp. 1164-1193, 2018.

[11] N. Anselmi, L. Poli, G. Oliveri, and A. Massa, "Iterative multi-resolution bayesian CS for microwave imaging," *IEEE Trans. Antennas Propag.*, vol. 66, no. 7, pp. 3665-3677, Jul. 2018.

[12] N. Anselmi, G. Oliveri, M. A. Hannan, M. Salucci, and A. Massa, "Color compressive sensing imaging of arbitrary-shaped scatterers," *IEEE Trans. Microw. Theory Techn.*, vol. 65, no. 6, pp. 1986-1999, Jun. 2017.

[13] N. Anselmi, G. Oliveri, M. Salucci, and A. Massa, "Wavelet-based compressive imaging of sparse targets" *IEEE Trans. Antennas Propag.*, vol. 63, no. 11, pp. 4889-4900, Nov. 2015.

[14] G. Oliveri, P.-P. Ding, and L. Poli, "3D crack detection in anisotropic layered media through a sparseness-regularized solver," *IEEE Antennas Wirel. Propag. Lett.*, vol. 14, pp. 1031-1034, 2015.

[15] L. Poli, G. Oliveri, P.-P. Ding, T. Moriyama, and A. Massa, "Multifrequency Bayesian compressive sensing methods for microwave imaging," *J. Opt. Soc. Am. A*, vol. 31, no. 11, pp. 2415-2428, 2014.

[16] G. Oliveri, N. Anselmi, and A. Massa, "Compressive sensing imaging of non-sparse 2D scatterers by a total-variation approach within the Born approximation," *IEEE Trans. Antennas Propag.*, vol. 62, no. 10, pp. 5157-5170, Oct. 2014.

[17] L. Poli, G. Oliveri, F. Viani, and A. Massa, "MT-BCS-based microwave imaging approach through minimum-norm current expansion," *IEEE Trans. Antennas Propag.*, vol. 61, no. 9, pp. 4722-4732, Sep. 2013.

[18] F. Viani, L. Poli, G. Oliveri, F. Robol, and A. Massa, "Sparse scatterers imaging through approximated multitask compressive sensing strategies," *Microwave Opt. Technol. Lett.*, vol. 55, no. 7, pp. 1553-1558, Jul. 2013.

[19] L. Poli, G. Oliveri, P. Rocca, and A. Massa, "Bayesian compressive sensing approaches for the reconstruction of two-dimensional sparse scatterers under TE illumination," *IEEE Trans. Geosci. Remote Sensing*, vol. 51, no. 5, pp. 2920-2936, May 2013.

[20] P. Rocca, N. Anselmi, M. A. Hannan, and A. Massa, "Conical frustum multi-beam phased arrays for air traffic control radars," *Sensors*, vol. 22, no. 19, 7309, pp. 1-18, 2022 (DOI: 10.3390/s22197309)

[21] F. Zardi, G. Oliveri, M. Salucci, and A. Massa, "Minimum-complexity failure correction in linear arrays via compressive processing," *IEEE Trans. Antennas Propag.*, vol. 69, no. 8, pp. 4504-4516, Aug. 2021.

[22] N. Anselmi, G. Gottardi, G. Oliveri, and A. Massa, "A total-variation sparseness-promoting method for the synthesis of contiguously clustered linear architectures," *IEEE Trans. Antennas Propag.*, vol. 67, no. 7, pp. 4589-4601, Jul. 2019.

[23] M. Salucci, A. Gelmini, G. Oliveri, and A. Massa, "Planar arrays diagnosis by means of an advanced Bayesian compressive processing," *IEEE Trans. Antennas Propag.*, vol. 66, no. 11, pp. 5892-5906, Nov. 2018.

[24] L. Poli, G. Oliveri, P. Rocca, M. Salucci, and A. Massa, "Long-Distance WPT Unconventional Arrays Synthesis," *J. Electromagn. Waves Appl.*, vol. 31, no. 14, pp. 1399-1420, Jul. 2017.

[25] G. Oliveri, M. Salucci, and A. Massa, "Synthesis of modular contiguously clustered linear arrays through a sparseness-regularized solver," *IEEE Trans. Antennas Propag.*, vol. 64, no. 10, pp. 4277-4287, Oct. 2016.

[26] M. Carlin, G. Oliveri, and A. Massa, "Hybrid BCS-deterministic approach for sparse concentric ring isophoric arrays," *IEEE Trans. Antennas Propag.*, vol. 63, no. 1, pp. 378-383, Jan. 2015.

[27] G. Oliveri, E. T. Bekele, F. Robol, and A. Massa, "Sparsening conformal arrays through a versatile BCS-based method," *IEEE Trans. Antennas Propag.*, vol. 62, no. 4, pp. 1681-1689, Apr. 2014.

[28] F. Viani, G. Oliveri, and A. Massa, “Compressive sensing pattern matching techniques for synthesizing planar sparse arrays,” *IEEE Trans. Antennas Propag*., vol. 61, no. 9, pp. 4577-4587, Sept. 2013.

[29] P. Rocca, M. A. Hannan, M. Salucci, and A. Massa, “Single-snapshot DoA estimation in array antennas with mutual coupling through a multi-scaling BCS strategy,” *IEEE Trans. Antennas Propag*., vol. 65, no. 6, pp. 3203-3213, Jun. 2017.

[30] M. Carlin, P. Rocca, G. Oliveri, F. Viani, and A. Massa, “Directions-of-arrival estimation through Bayesian Compressive Sensing strategies,” *IEEE Trans. Antennas Propag*., vol. 61, no. 7, pp. 3828-3838, Jul. 2013.

[31] M. Carlin, P. Rocca, G. Oliveri, and A. Massa, “Bayesian compressive sensing as applied to directions-of-arrival estimation in planar arrays," *J. Electromagn. Waves Appl.*, vol.2013, pp.1-12, 2013 (DOI :10.1155/2013/245867).